

Generalized Neighbor-Interaction Models Induced by Nonlinear Lattices.

F. Kh. Abdullaev^{1,*}, Yu. V. Bludov^{2,†}, S. V. Dmitriev^{3,‡}, P. G. Kevrekidis^{4,§} and V. V. Konotop^{2,5,¶}

¹*Instituto de Física Teórica, UNESP, Rua Pamplona, 145, Sao Paulo, Brasil*

²*Centro de Física Teórica e Computacional, Universidade de Lisboa,*

Complexo Interdisciplinar, Avenida Professor Gama Pinto 2, Lisboa 1649-003, Portugal

³*General Physics Department, Altai State Technical University, 656038 Barnaul, Russia*

⁴*Department of Mathematics and Statistics, University of Massachusetts, Amherst, MA 01003 USA*

⁵*Departamento de Física, Universidade de Lisboa,*

Campo Grande, Ed. C8, Piso 6, Lisboa 1749-016, Portugal

It is shown that the tight-binding approximation of the nonlinear Schrödinger equation with a periodic linear potential and periodic in space nonlinearity coefficient gives rise to a number of nonlinear lattices with complex, both linear and nonlinear, neighbor interactions. The obtained lattices present non-standard possibilities, among which we mention a quasi-linear regime, where the pulse dynamics obeys essentially the linear Schrödinger equation. We analyze the properties of such models both in connection with their modulational stability, as well as in regard to the existence and stability of their localized solitary wave solutions.

PACS numbers:

I. INTRODUCTION

It is generally recognized that mapping of a nonlinear evolution problem, described by a partial differential equation, into a simplified lattice, representing a set of coupled ordinary differential equations, appears to be a useful tool either for numerical (or semi-analytical in the appropriate limits) study of the dynamics or for bringing intuitive understanding of the factors dominating the behavior of the systems. Examples of such approach are well known for a long time in solid state physics [1] (the description of an electron in a crystal in the tight-binding approximation), in optics [2] (the description of the electric field in arrays of waveguides), and more recently in the mean-field theory of Bose-Einstein condensates loaded in optical lattices (see e.g. [3, 4] for relevant reviews). In all mentioned cases, the periodicity is usually associated with the linear properties of the system and the respective dynamics is approximately described by the discrete nonlinear Schrödinger (DNLS) equation.

On the other hand, there has recently been an increasing interest in studying nonlinear models, where the nonlinearity is also periodically modulated in space. Applications of such models extend from the propagation of electromagnetic waves in stratified media [5] to condensates of bosons [6] and condensates of boson-fermion mixtures [7] in optical lattices. It turned out that the spatially dependent nonlinearity may dramatically change properties of the system, in particular the regions of existence of coherent localized structures and especially their corresponding stability properties.

Natural questions that arise in this context are the mapping of the respective evolution equation into nonlinear lattice and the description of the existence, stability, and dynamics properties of such lattices. In the present paper we consider both of these issues. While the first issue is technical and can be straightforwardly addressed by means of the Wannier function expansion, as it was suggested in [8], the study of the properties of the emerging lattices is a much richer problem in the present setting; its richness stems from the fact that spatially dependent nonlinearity gives rise to complex nonlinear inter-site interactions. Such additional forms of nonlinearity as the ones extracted below can significantly change the dynamical properties of the discrete system as it was shown in earlier research devoted to the spin waves in magnetic systems [9], electromagnetic waves in waveguide arrays [10, 11] and to applications to arrays of Bose-Einstein condensates [12]. In the above mentioned studies of nonlinear lattices, however, one common feature was of crucial importance – that was the presence of dominant (or at least significant) on-site nonlinearity, which e.g., in the case of a BEC loaded in an optical lattice is typically about two orders of magnitude larger than the hopping nonlinearity. In the present paper, we systematically derive and consider a far more general class of lattice evolution equations, including the cases where the on-site nonlinearity is exactly zero.

The organization of the paper is as follows. In Sec. II we deduce the relevant lattice dynamical models with inter-site nonlinearity starting with the evolution equation of the nonlinear Schrödinger (NLS) type with a spatially periodic potential and periodic nonlinearity. In Sec. III, we conduct the modulational stability analysis of the derived models. In sections IV and V, we examine the respective dynamical properties of the derived quasi-linear and nonlinear models, while Sec. VI summarizes our findings and presents our conclusions, as well as directions of potential future interest.

*Electronic address: fatkh@uzsci.net

†Electronic address: bludov@cii.fc.ul.pt

‡Electronic address: dmitriev.sergey.v@gmail.com

§Electronic address: kevrekid@math.umass.edu

¶Electronic address: konotop@cii.fc.ul.pt

II. MODEL EQUATIONS

A. One-band approximation

We start with the one-dimensional NLS equation

$$i\frac{\partial\psi}{\partial t} = -\frac{\partial^2\psi}{\partial x^2} + \mathcal{U}(x)\psi + \mathcal{G}(x)|\psi|^2\psi, \quad (1)$$

where $\mathcal{U}(x)$ and $\mathcal{G}(x)$ are the coordinate-dependent linear and nonlinear potentials respectively, both considered to be π -periodic functions: $\mathcal{U}(x) = \mathcal{U}(x + \pi)$ and $\mathcal{G}(x) = \mathcal{G}(x + \pi)$. We concentrate on the cases where the linear potential is an even function $\mathcal{U}(x) = \mathcal{U}(-x)$, while the nonlinearity may be either even or odd: $\mathcal{G}(x) = \sigma\mathcal{G}(-x)$ (hereafter $\sigma = \pm 1$).

In order to map Eq. (1) into a lattice equation we follow [8]. To this end, we introduce the linear eigenvalue problem

$$-\frac{d^2\varphi_{\alpha q}(x)}{dx^2} + \mathcal{U}(x)\varphi_{\alpha q}(x) = \mathcal{E}_{\alpha q}\varphi_{\alpha q}(x) \quad (2)$$

where $\varphi_{\alpha q}(x)$ is a Bloch function, $\alpha \geq 1$ and q stand for the band number and for the wavenumber in the first Brillouin zone: $q \in [-1, 1]$, and define the Wannier functions

$$w_{n\alpha}(x) = \frac{1}{\sqrt{2}} \int_{-1}^1 \varphi_{\alpha q}(x) e^{-i\pi n q} dq, \quad (3)$$

which constitute an orthonormal set of real and exponentially decaying functions [13].

We seek the solution of Eq. (1) in the form of a series

$$\psi(x, t) = \sum_{n, \alpha} c_{n\alpha}(t) w_{n\alpha}(x). \quad (4)$$

For the next consideration we notice that the Wannier functions of α -th band possess either even or odd parity $w_{0\alpha}(x) = (-1)^{1+\alpha} w_{0\alpha}(-x)$ and are characterized by the property $w_{n\alpha}(x) = w_{0\alpha}(x - n\pi)$.

Now we make the most crucial approximation of our model, namely that the continuum Eq. (1) can be accurately described within the one-band approximation. As it was shown in [8], this assumption fails to describe the original continuous model when one studies dynamical processes associated with the generation of the frequencies belonging to the higher bands. However, it is reasonably accurate in describing static solutions (in particular, localized modes) as well as their stability. Also, the lattices of generalized neighbor interactions derived below within the framework of the one-band approximation, are of interest in their own right, per their particularities and differences in comparison to other models of similar type; cf. [10, 11].

We thus assume that only one band, say α -th one, is populated. Now, substituting the expansion (4) in Eq.

(1) we arrive at the equation (see [3, 8] for more details)

$$i\dot{c}_{n\alpha} - c_{n\alpha}\omega_{0\alpha} - (c_{n-1,\alpha} + c_{n+1,\alpha})\omega_{1\alpha} - \sum_{n_1, n_2, n_3} c_{n_1\alpha} \bar{c}_{n_2\alpha} c_{n_3\alpha} W_{\alpha\alpha\alpha\alpha}^{nn_1n_2n_3} = 0, \quad (5)$$

where

$$W_{\alpha\alpha_1\alpha_2\alpha_3}^{nn_1n_2n_3} = \int_{-\infty}^{\infty} \mathcal{G}(x) w_{n\alpha}(x) w_{n_1\alpha_1}(x) w_{n_2\alpha_2}(x) w_{n_3\alpha_3}(x) dx \quad (6)$$

are the nonlinear overlap integrals, $\omega_{n\alpha}$ are the coefficients of the Fourier series expansion of the eigenvalue $\mathcal{E}_{\alpha q}$:

$$\mathcal{E}_{\alpha q} = \sum_n \omega_{n\alpha} e^{i\pi n q}, \quad \omega_{n\alpha} = \frac{1}{2} \int_{-1}^1 \mathcal{E}_{\alpha q} e^{-i\pi n q} dq; \quad (7)$$

the overbar stands for complex conjugation, and an overdot stands for the derivative with respect to time. In Eq. (5) we have taken into account that in a general situation, for a periodic potential $\mathcal{U}(x)$ of rather large amplitude, the lowest bands are very narrow, and hence the Fourier coefficients $\omega_{n\alpha}$ decay rapidly with increasing n (so that $|\omega_{0\alpha}| \gg |\omega_{1\alpha}| \gg |\omega_{2\alpha}|$), which, in turn, allows us to neglect the coefficients $\omega_{n\alpha}$ with $n \geq 2$.

For the lowest bands the Wannier functions are well localized on the scale of one lattice period (and can be reasonably well approximated by the eigenstates of the linear oscillator) and thus the overlap integrals involving next-nearest neighbors (i.e., lattice minima separated by two lattice maxima) are negligibly small. This allows us to drop also the terms involving $W_{\alpha_1\alpha_2\alpha_3\alpha_4}^{n_1n_2n_3n_4}$ with at least one pair of the upper indices satisfying $|n_j - n_k| \geq 2$. We however emphasize, that it is of crucial importance to leave the nonlinear terms with hopping between the neighbor sites, which for specific choices of the nonlinear interactions $\mathcal{G}(x)$ can be comparable with or even stronger than the on-site nonlinearity (see below).

Now we use the symmetry of the integrals W with respect to permutations of the indices and introduce

$$\begin{aligned} W_0 &= W_{\alpha\alpha\alpha\alpha}^{nnnn} = W_{\alpha\alpha\alpha\alpha}^{0000}, \\ W_1 &= W_{\alpha\alpha\alpha\alpha}^{n,n-1,n-1,n-1} = \sigma W_{\alpha\alpha\alpha\alpha}^{n,n,n,n-1} = W_{\alpha\alpha\alpha\alpha}^{1000}, \\ W_2 &= W_{\alpha\alpha\alpha\alpha}^{n,n,n-1,n-1} = W_{\alpha\alpha\alpha\alpha}^{1100}, \end{aligned} \quad (8)$$

where $\sigma = 1$ and $\sigma = -1$ for $\mathcal{G}(x)$ even and odd and

$$W_j = \int_{-\infty}^{\infty} \mathcal{G}(x) w_{1\alpha}^j(x) w_{0\alpha}^{4-j}(x) dx \quad j = 0, 1, 2. \quad (9)$$

In the case of odd nonlinearity ($\sigma = -1$) the terms W_0 and W_2 are always equal to zero due to the fact that the integrand in (9) is odd with respect to the points $X = 0$ and $X = \pi/2$, correspondingly. We thus arrive at the equation

$$\begin{aligned} i\dot{c}_n &= \omega_0 c_n + \omega_1 (c_{n-1} + c_{n+1}) + W_0 |c_n|^2 c_n \\ &+ W_1 (|c_{n-1}|^2 c_{n-1} + \sigma \bar{c}_{n-1} c_n^2 + 2\sigma |c_n|^2 c_{n-1} \\ &+ 2|c_n|^2 c_{n+1} + \bar{c}_{n+1} c_n^2 + \sigma |c_{n+1}|^2 c_{n+1}) \\ &+ W_2 (2|c_{n-1}|^2 c_n + \bar{c}_n c_{n-1}^2 + \bar{c}_n c_{n+1}^2 + 2|c_{n+1}|^2 c_n), \end{aligned} \quad (10)$$

where we have dropped the zone index α (e.g. $c_{n,\alpha}$ is redefined as c_n , etc.)

Eq. (10) is the main discrete model studied in the present paper. We notice that it has a Hamiltonian structure: $i\dot{c}_n = \partial H / \partial \bar{c}_n$ with the Hamiltonian

$$H = \sum_n \left[\omega_0 |c_n|^2 + \omega_1 (c_{n-1} \bar{c}_n + \bar{c}_{n-1} c_n) + \frac{W_0}{2} |c_n|^4 + W_1 (|c_{n-1}|^2 + \sigma |c_n|^2) (c_n \bar{c}_{n-1} + \bar{c}_n c_{n-1}) + 2W_2 |c_{n-1}|^2 |c_n|^2 + \frac{W_2}{2} (c_n^2 \bar{c}_{n-1}^2 + \bar{c}_n^2 c_{n-1}^2) \right] \quad (11)$$

and with the standard Poisson brackets. Another integral of motion is the sum $N = \sum_n |c_n|^2$, reflecting the conservation of the ‘‘number of atoms’’ (in keeping with the BEC motivation of our analysis) of the original Eq. (1).

B. Particular cases

The deduced model (10) allows for a number of interesting particular cases. First of all, however we notice that in the case of odd nonlinearity function, i.e., for $\sigma = -1$, neither purely even ($c_n = c_{-n}$), nor purely odd ($c_n = -c_{-n}$) solutions can exist. This follows directly from the symmetry of Eq. (10) [or Eq. (1)].

For illustration of the localized solutions we use the potential $\mathcal{U}(X) = -3 \cos(2X)$ (both for the detailed calculations of this section, and for the numerical simulations of the following sections). Also we restrict our considerations to the first band, i.e. we take $\alpha = 1$. In that case, the linear overlap coefficients for the first band are computed as $\omega_0 \approx -0.839$, $\omega_1 \approx -0.051$, and $\omega_2 \approx 0.002$ [23].

One can distinguish five cases as follows:

Case 1: $W_0 = W_1 = W_2 = 0$. This is a quasi-linear case, which is made possible, for example by an odd nonlinearity ($\sigma = -1$) of the form

$$\mathcal{G}(x) = \sin(2x) - 1.3706 \sin(4x) \quad (12)$$

(obviously a number of possible realizations of this and other cases reported below is naturally unlimited). Our approach both in this example and below is motivated by the nature of the lattice that we wish to construct (i.e., by the type of overlap integral that we wish to preserve or eliminate). For instance, in this example, the odd nonlinearity guarantees that $W_0 = W_2 = 0$, while the expression of Eq. (12) uses one tunable parameter (the amplitude of the second harmonic) to achieve $W_1 = 0$.

Case 2: $W_0 = W_2 = 0$, $W_1 \neq 0$, is achieved e.g. by choosing

$$\mathcal{G}(x) = 10 \sin(2x) \quad (13)$$

($\sigma = -1$). Now the lattice model (10) is reduced to

$$i\dot{c}_n = \omega_0 c_n + \omega_1 (c_{n-1} + c_{n+1}) + W_1 (|c_{n-1}|^2 c_{n-1} - \bar{c}_{n-1} c_n^2 - 2|c_n|^2 c_{n-1} + 2|c_n|^2 c_{n+1} + \bar{c}_{n+1} c_n^2 - |c_{n+1}|^2 c_{n+1}), \quad (14)$$

and in the case at hand $W_1 \approx 0.045$.

Alternatively, this case can be realized by choosing even nonlinearity ($\sigma = 1$)

$$\mathcal{G}(x) = 0.0275 + 4.809 \cos(2x) - 10 \cos(4x). \quad (15)$$

Now $W_1 \approx 0.012$ and the lattice equation reads:

$$i\dot{c}_n = \omega_0 c_n + \omega_1 (c_{n-1} + c_{n+1}) + W_1 (|c_{n-1}|^2 c_{n-1} + \bar{c}_{n-1} c_n^2 + 2|c_n|^2 c_{n-1} + 2|c_n|^2 c_{n+1} + \bar{c}_{n+1} c_n^2 + |c_{n+1}|^2 c_{n+1}). \quad (16)$$

Case 3: $W_0 = W_1 = 0$, $W_2 \neq 0$ is obtained, for instance, for the even nonlinearity ($\sigma = 1$)

$$\mathcal{G}(x) = -23.836 + 48.882 \cos(2x) - 37.778 \cos(4x), \quad (17)$$

for which $W_2 \approx -0.0136$. The model (10) is now simplified

$$i\dot{c}_n = \omega_0 c_n + \omega_1 (c_{n-1} + c_{n+1}) + W_2 (2|c_{n-1}|^2 c_n + \bar{c}_n c_{n-1}^2 + \bar{c}_n c_{n+1}^2 + 2|c_{n+1}|^2 c_n). \quad (18)$$

Case 4: $W_0 = 0$, $W_{1,2} \neq 0$ can be achieved by using an even nonlinearity ($\sigma = 1$)

$$\mathcal{G}(x) = 7.795 - 10 \cos(2x). \quad (19)$$

Now the overlap integrals are as follows $W_1 \approx 0.0148$ and $W_2 \approx 0.0045$. The lattice model then reads

$$i\dot{c}_n = \omega_0 c_n + \omega_1 (c_{n-1} + c_{n+1}) + W_1 (|c_{n-1}|^2 c_{n-1} + \bar{c}_{n-1} c_n^2 + 2|c_n|^2 c_{n-1} + 2|c_n|^2 c_{n+1} + \bar{c}_{n+1} c_n^2 + |c_{n+1}|^2 c_{n+1}) + W_2 (2|c_{n-1}|^2 c_n + \bar{c}_n c_{n-1}^2 + \bar{c}_n c_{n+1}^2 + 2|c_{n+1}|^2 c_n). \quad (20)$$

Case 5: $|W_1|, |W_2| \ll |W_0|$ is the standard case of the on-site nonlinearity (the DNLS equation):

$$i\dot{c}_n = \omega_0 c_n + \omega_1 (c_{n-1} + c_{n+1}) + W_0 |c_n|^2 c_n. \quad (21)$$

This form of the lattice dynamical model is obtained for generic nonlinearities, Eq.(21) is well studied in the literature (see e.g. [14]) and that is why it will not be addressed in this paper.

III. MODULATIONAL INSTABILITY

As it is customary we start with the analysis of the modulational instability of plane-wave solutions of Eq. (10) (for a general study of the modulational instability of the plane wave background in the DNLS-type equations see e.g. [15, 16, 17]). This stability analysis is performed not only because it is of interest in its own right but also because the solitary wave solutions that we plan on constructing for the above presented lattices should be

produced on a dynamically stable background. Using the plane wave solution of the form:

$$c_n = F e^{i(qn - \omega t)}, \quad (22)$$

where F is a constant amplitude, we obtain the dispersion relation (in the absence of the previously considered cubic onsite terms)

$$\omega = \omega_0 + 2\omega_1 \cos(q) + 4W_1 F^2 (\sigma + 1) \cos(q) + 2W_2 F^2 [2 + \cos(2q)]. \quad (23)$$

To examine the linear stability, we perturb the plane wave solution in the form:

$$c_n = (F + A e^{i(Qn - \Omega t)} + \bar{B} e^{-i(Qn - \Omega t)}) e^{i(qn - \omega t)}, \quad (24)$$

with $|A|, |B| \ll |F|$ and linearize with respect to A and B . As a result we obtain two branches of the linear excitations $\Omega_{1,2}(Q)$:

$$\Omega_{1,2} = M_- \pm \sqrt{(M_+ - D)^2 - F^4 \Delta}, \quad (25)$$

where

$$\begin{aligned} D &= \omega - \omega_0 - 4W_1(1 + \sigma)F^2 \cos(q) - 4W_2 F^2 (\cos(Q) + 1), \\ M_- &= -2(\omega_1 + 2W_1(1 + \sigma)F^2) \sin(Q) \sin(q) - 4W_2 F^2 \sin(Q) \sin(2q), \\ M_+ &= 2(\omega_1 + 2W_1(1 + \sigma)F^2) \cos(Q) \cos(q) + 4W_2 F^2 \cos(Q) \cos(2q), \\ \Delta &= 4[W_1(1 + \sigma)(1 + \cos(Q)) \cos(q) + W_2(2 \cos(Q) + \cos(2q))]^2 + 4(1 - \sigma)^2 \sin^2(q) W_1^2 (1 - \cos(Q))^2. \end{aligned}$$

Let us consider different special cases for $\sigma = -1$ (the case $\sigma = 1$ is investigated in [10]).

a. Homogeneous background is described by $q = 0$. Now the two branches of the solutions collapse and the dispersion relation acquires the form

$$\begin{aligned} \Omega^2 &= 16(\omega_1 + 2W_2 F^2) \sin^2\left(\frac{Q}{2}\right) \\ &\times \left[(\omega_1 + 6W_2 F^2) \sin^2\left(\frac{Q}{2}\right) - 3W_2 F^2 \right]. \quad (26) \end{aligned}$$

The carrier field is stable if and only if the two following conditions are satisfied

$$\begin{aligned} (\omega_1 + 2W_2 F^2) W_2 &\leq 0, \\ (\omega_1 + 2W_2 F^2) (\omega_1 + 3W_2 F^2) &\geq 0, \quad (27) \end{aligned}$$

where the first of these conditions demands non-negativity of the coefficient k in the expansion of Eq. (26) of the form of $\Omega^2(Q) = kQ^2$, which is valid for small Q . The second condition demands non-negativity of $\Omega^2(Q)$ at the zone boundary, $Q = \pi$.

We point out that the long wavelength excitations' group velocity dispersion is given by

$$\left. \frac{\partial^2 \Omega}{\partial Q^2} \right|_{Q=0} = 2W_2 [2W_2 F^4 + (8W_2 - 6 + \omega_1) F^2 + 4\omega_1] \quad (28)$$

and takes zero values for

$$F = \left\{ \frac{6 - \omega_1 - 8W_2}{4W_2} \pm \sqrt{\left(\frac{6 - \omega_1 - 8W_2}{4W_2} \right)^2 - \frac{2\omega_1}{W_2}} \right\}^{1/2}.$$

This last condition determines the domain of the parameters where shock waves can be observed [18].

b. Staggered background corresponds to $q = \pi$. The dispersion relation is

$$\begin{aligned} \Omega^2 &= 16(\omega_1 - 2W_2 F^2) \sin^2\left(\frac{Q}{2}\right) \\ &\times \left[(\omega_1 - 6W_2 F^2) \sin^2\left(\frac{Q}{2}\right) + 3W_2 F^2 \right]. \quad (29) \end{aligned}$$

Similar to (27) we introduce stability criteria in the form

$$\begin{aligned} (\omega_1 - 2W_2 F^2) W_2 &\geq 0, \\ (\omega_1 - 2W_2 F^2) (\omega_1 - 3W_2 F^2) &\geq 0. \quad (30) \end{aligned}$$

Note that the dispersion relations for $q = 0, \pi$ do not depend on the coefficient W_1 .

c. Phase alternating background where $q = \pi/2$. The dispersion relation is

$$\begin{aligned} \Omega_{1,2} &= -2\omega_1 \sin(Q) \pm \\ 4\sqrt{2} F^2 \sin\left(\frac{Q}{2}\right) &\sqrt{(W_2^2 + W_1^2) \cos(Q) - W_1^2}. \quad (31) \end{aligned}$$

The condition for the presence of modulational instability in this case is

$$\cos(Q) < \frac{W_1^2}{W_1^2 + W_2^2}. \quad (32)$$

IV. QUASI-LINEAR MODEL (CASE 1)

Let us now turn to the quasi-linear model of Case 1. We notice that the term ‘‘quasi-linear’’ is used in order to emphasize the existence of solely higher order contributions from more distant neighbors which are small but not necessarily zero. This provides us with an excellent benchmark of our derivation since in the discrete linear case, the dynamical equation can be solved explicitly and subsequently compared to the full results of the original partial differential equation (for which the discrete model was developed as an approximation). In particular, it is well-known that the linear discrete case, with a compactum of initial data $c_n(0) = A\delta_{n0}$ has a solution of the form

$$c_n(t) = A (-i)^n \exp(-i\omega_0 t) J_n(2\omega_1 t) \quad (33)$$

where J_n is the Bessel function of order n .

We have tested this analytical prediction of the *discrete model* in the partial differential equation (1) with the “nonlinear potential” of Eq. (12). The results of our numerical simulations can be found in Fig. 1, which highlights the excellent agreement between the analytical and the numerical results. This also serves to showcase the accuracy of the reduction via the tight-binding approximation of the original partial differential equation. We will hereafter focus more on the details of these discrete models and of their solitary wave solutions.

The remarkable accuracy of the tight-binding model in the case at hand can be easily understood. Indeed, we are dealing with a perfect lattice (i.e. having no defects). Inter-band transitions, which are the cause of the failure of the one-band approximation when they exist, are only due to the nonlinear coupling of bands, and exactly this factor is anomalously small for the chosen nonlinearity. The first indication on this fact is given by the zero contributions of $W_{0,1,2}$. Next, due to the symmetry of the Wannier functions, and the symmetry of the nonlinearity, one concludes that $W_{\alpha\alpha\beta\beta}^{nnnn} = 0$ for all α and β , i.e., there exists no tunneling between the same sites of two different bands. Even more generally (also due to the symmetry), $W_{\alpha,\beta,\beta,\alpha+2\gamma}^{n,n-m,n+m,n} = 0$ (for arbitrary integers β, γ, n and m). For completeness we have checked the numerical values of the other inter-band overlap integrals for the three lowest bands. The integrals greater than 0.01 are as follows (the ones obtained by the symmetry reductions are not shown) $W_{2111}^{0000} = 0.0465$, $W_{2221}^{0000} = -0.1360$, $W_{2211}^{1000} = -0.0228$, $W_{3111}^{1000} = -0.0432$, $W_{3311}^{1000} = -0.0301$, $W_{1333}^{1000} = -0.0117$. The coefficients describing energy transfer from the first to the second and the third bands are $W_{2111}^{0000} = 0.0465$, $W_{3111}^{0000} = 0$, $W_{2111}^{1000} = 0.0077$, $W_{3111}^{1000} = -0.0432$, $W_{2111}^{1100} = 0.0004$, $W_{3111}^{1100} = 0.0011$, i.e., either have relatively small value or are identically zero. This explains the high accuracy of the one-band approximation.

Finally we notice, that in the case at hand the dispersion relation (25) takes the form independent of the wave amplitude F

$$\Omega = \pm 2\omega_1 [\cos(q) - \cos(Q \mp q)], \quad (34)$$

which is the dispersion relation for linear phonons, and hence no instabilities can occur.

V. NONLINEAR MODELS (CASES 2 AND 3)

The above confirmation of the high accuracy of the tight-binding model for the description of the pulse dynamics motivated us to study the coherent structure solutions of Eq. (10) and their properties for the Cases 2 and 3 singled out in Sec. II B. It is convenient to join the equations of the Cases 2 and 3 and to consider for $\sigma = 1$

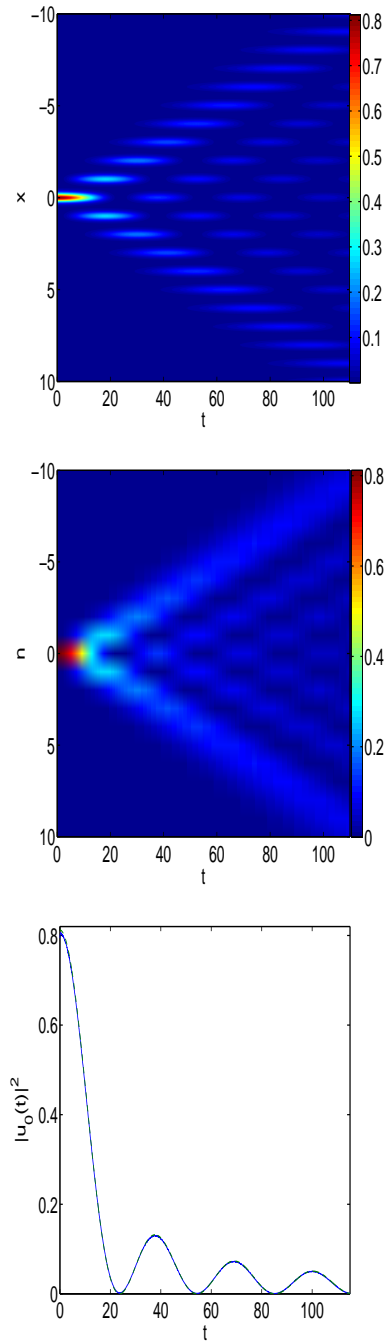


FIG. 1: The top and middle panel show the space-time contour plot of the solution in the PDE of Eq. (1) [top panel] and the discrete model analytical prediction (33) [middle panel]. In the latter case, space is normalized over the period of the linear potential, so that it can be compared with the lattice results. To accentuate the excellent agreement between analytical and numerical results, the bottom panel shows the time evolution of the amplitude at the central site of the configuration compared between the PDE numerical result (solid line) and the discrete equation analytical result of (33) (dashed line). The two are practically *indistinguishable*.

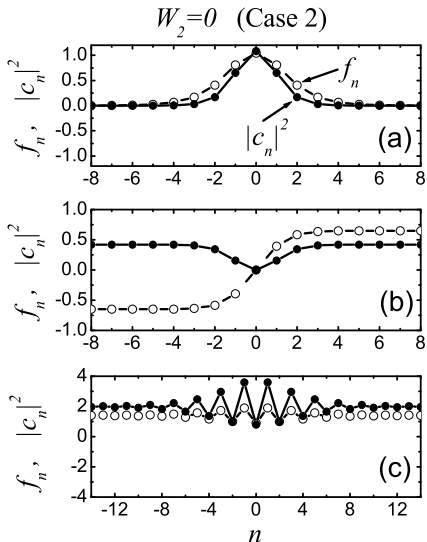


FIG. 2: Equilibrium soliton solutions found in the Case 2 ($W_2 = 0$): (a) pulse, (b) kink, and (c) anti-dark structure with oscillatory wave structure around the background, hereafter termed wave. On-site structures are presented here, but inter-site ones can also be constructed. Solutions in (a) and (b) can be stable but we were unable to find a stable structure of the form presented in (c) (see Sec. V C). Model parameters corresponding to panels (a) to (c) are depicted by dots in Fig. 3 marked by the capital letters A to C, respectively. Parameters are: (a) $W_1 = -0.0112$, $\omega = -0.99$, (b) $W_1 = 0.0112$, $\omega = -0.9$, (c) $W_1 = 0.0112$, $\omega = -0.75$.

the model

$$\begin{aligned}
 i\dot{c}_n &= \omega_0 c_n + \omega_1 (c_{n-1} + c_{n+1}) \\
 &+ W_1 (|c_{n-1}|^2 c_{n-1} + \bar{c}_{n-1} c_n^2 + 2|c_n|^2 c_{n-1} \\
 &+ 2|c_n|^2 c_{n+1} + \bar{c}_{n+1} c_n^2 + |c_{n+1}|^2 c_{n+1}) \\
 &+ W_2 (2|c_{n-1}|^2 c_n + \bar{c}_n c_{n-1}^2 + \bar{c}_n c_{n+1}^2 + 2|c_{n+1}|^2 c_n). \quad (35)
 \end{aligned}$$

Let us seek stationary solutions of Eq. (35) of the form

$$c_n(t) = f_n e^{-i\omega t}, \quad (36)$$

with real f_n . Using this ansatz, we obtain the equation for the amplitudes

$$\begin{aligned}
 (\omega_0 - \omega) f_n + \omega_1 (f_{n-1} + f_{n+1}) \\
 + W_1 [f_{n-1}^3 + f_{n+1}^3 + 3f_n^2 (f_{n+1} + f_{n-1})] \\
 + 3W_2 f_n (f_{n-1}^2 + f_{n+1}^2) = 0. \quad (37)
 \end{aligned}$$

We attempt to find the pulse (bright soliton) and kink (dark soliton) solutions. Our strategy in searching for these solutions will be as follows. We will first formulate the necessary conditions for the existence of the soliton solutions considering their carrier constant-amplitude field and also the soliton tail solutions. This

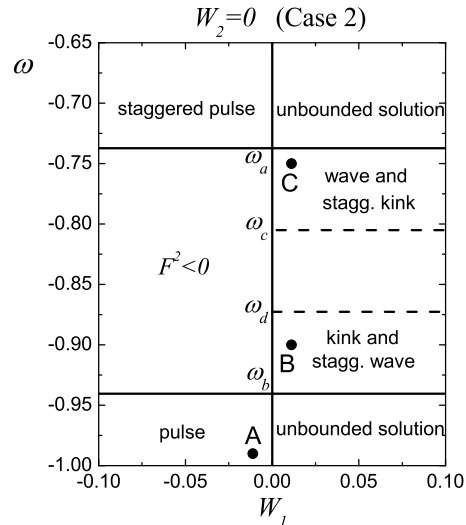


FIG. 3: Parameter plane (W_1, ω) in the Case 2 ($W_2 = 0$) with indicated regions of existence of three types of solitons shown in Fig. 2 and their staggered analogues. The pulse solution exists for $W_1 < 0$ and $\omega < \omega_b$, while the staggered pulse for $W_1 < 0$ and $\omega > \omega_a$. The kink and staggered wave can exist for $W_1 > 0$ and $\omega_b < \omega < \omega_c$, while the staggered kink and the wave for $W_1 > 0$ and $\omega_d < \omega < \omega_a$. The values of special frequencies ω_a to ω_d are given by Eq. (46) and Eq. (47).

will narrow the domain of parameters where such solutions can be expected. Then, we will attempt to construct the desired soliton solutions and subsequently study their stability.

The staggered and non-staggered stationary solutions are connected by the following symmetry relation [19]: if f_n is a solution of Eq. (37) for definite W_1, W_2 , and $\omega < \tilde{\omega}_0$ ($\omega > \omega_0$), then $(-1)^n f_n$ is a solution for $\tilde{W}_1 = W_1, \tilde{W}_2 = -W_2$, and $\tilde{\omega} = 2\omega_0 - \omega > \omega_0$ ($\tilde{\omega} < \omega_0$). We also note that the stability analysis of any stationary solution can also be done, without loss of generality, for only, say, non-staggered carrier field. This is so because the dynamics in the vicinity of the stationary solution is governed by Eq. (51) (see below) which is invariant with respect to the following transformation: $\epsilon_n \rightarrow (-1)^n \epsilon_n$, $f_n \rightarrow (-1)^n f_n$, $\omega \rightarrow 2\omega_0 - \omega$, $W_2 \rightarrow -W_2$, and $t \rightarrow -t$. Bearing this in mind, in the following we will discuss only stationary solutions with a non-staggered background.

A. Constant amplitude solution and soliton tails

A pulse solution must satisfy the boundary conditions $|c_n|^2 \rightarrow 0$ for $n \rightarrow \pm\infty$, while for the kink solution one must have $|c_n|^2 \rightarrow F^2 > 0$ for $n \rightarrow \pm\infty$. Thus, the existence and stability of the carrying field solution, described by formula (22) with real F , is a necessary con-

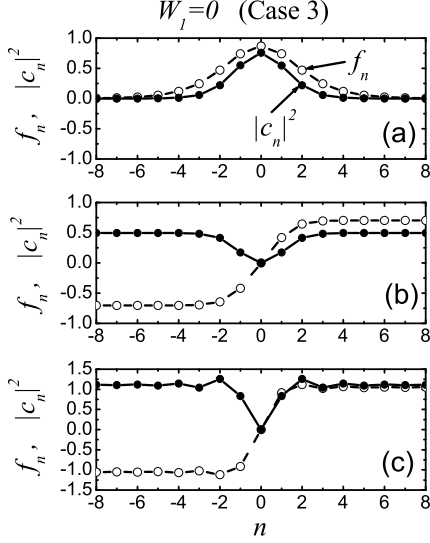


FIG. 4: Equilibrium soliton solutions obtained in Case 3 with $W_1 = 0$: (a) pulse, (b) kink, and (c) kink with oscillatory tail, called oscillatory kink. On-site structures are presented here, but inter-site ones can also be constructed. All these solutions can be stable, as it will be shown in Sec. V C. Model parameters corresponding to panels (a) to (c) are depicted by dots in Fig. 5 marked by the capital Latin letters A to C, respectively. Parameters are: (a) $W_2 = -0.0136$, $\omega = -0.9704$, (b) $W_2 = 0.0136$, $\omega = -0.9$, (c) $W_2 = 0.0136$, $\omega = -0.85$.

dition for the existence and stability of the soliton solutions.

One always has the trivial solution $F = 0$ and from the expression (23) one can have two nonzero solutions with

$$F^2 = \frac{\omega - \omega_0 - 2\omega_1}{8W_1 + 6W_2}, \quad (38)$$

if the expression in the right-hand side of Eq. (38) is positive. In the case $8W_1 + 6W_2 = 0$, F can be arbitrary if $\omega = \omega_0 + 2\omega_1$, but we will not study this very special case.

Substituting Eq. (38) into Eq. (25) we obtain the spectrum of the carrier field with $F^2 > 0$, whose stability criteria (in full analogy with Sec. III) are

$$\begin{aligned} [W_1(\omega - \omega_0 + 2\omega_1) + W_2(\omega - \omega_0 + \omega_1)] \times \\ (4W_1 + 3W_2)(\omega - \omega_0 - 2\omega_1) \leq 0, \\ [W_1(\omega - \omega_0 + 2\omega_1) + W_2(\omega - \omega_0 + \omega_1)] \times \\ [2W_1(\omega - \omega_0 + 2\omega_1) + 3W_2(\omega - \omega_0)] \geq 0. \end{aligned} \quad (39)$$

From the asymptotic properties mentioned above, one can express the soliton tails as

$$f_n \sim F + \xi_n \quad (40)$$

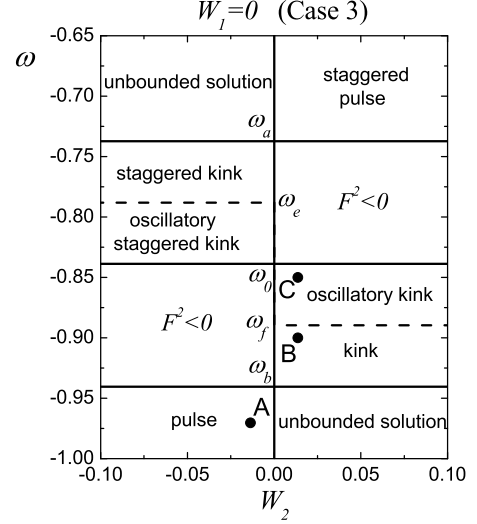


FIG. 5: Parameter plane (W_2, ω) in Case 3 ($W_1 = 0$) with indicated regions of existence of three types of solitons shown in Fig. 4 and their staggered analogues. The pulse exists for $W_2 < 0$ and $\omega < \omega_b$, while the staggered pulse for $W_2 > 0$ and $\omega > \omega_a$. The kink exists for $W_2 > 0$ and $\omega_b < \omega < \omega_f$, while the staggered kink for $W_2 < 0$ and $\omega_e < \omega < \omega_a$. Finally, the oscillatory kink exists for $W_2 > 0$ and $\omega_f < \omega < \omega_0$, while the oscillatory staggered kink for $W_2 < 0$ and $\omega_0 < \omega < \omega_e$. Values of special frequencies are given by Eq. (46) and Eq. (48).

at $|n| \rightarrow \infty$, where small ξ_n are real and are independent on t . Substituting Eq. (40) into Eq. (37) and linearizing with respect to ξ_n one obtains

$$\gamma\xi_{n-1} + \beta\xi_n + \gamma\xi_{n+1} = 0, \quad (41)$$

with

$$\begin{aligned} \beta &= \omega_0 - \omega + 12W_1F^2 + 6W_2F^2, \\ \gamma &= \omega_1 + 6W_1F^2 + 6W_2F^2. \end{aligned} \quad (42)$$

Seeking solutions to Eq. (41) in the form

$$\xi_n \sim C_{\pm} z^n, \quad n \rightarrow \pm\infty$$

with complex z , we come to the characteristic equation

$$\gamma z^2 + \beta z + \gamma = 0. \quad (43)$$

Thus, z is one of the roots $z_{1,2}$

$$z_1 = \frac{1}{z_2} = -\frac{\beta}{2\gamma} + \sqrt{\frac{\beta^2}{4\gamma^2} - 1} \quad (44)$$

providing $|\xi_n| \rightarrow 0$ as $|n| \rightarrow \infty$.

For the soliton, which is either a homoclinic or a heteroclinic of the map, generated by Eq. (37), $\xi_n \equiv 0$ must

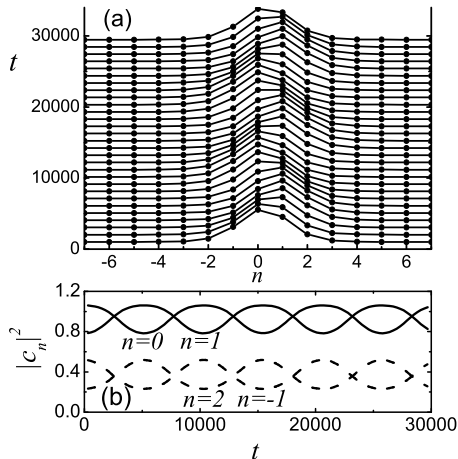


FIG. 6: Pulse in Case 2 ($W_2 = 0$). (a) Space-time evolution of $|c_n(t)|^2$ showing the dynamics of the pulse placed at $t = 0$ asymmetrically with respect to the lattice. The pulse undergoes periodic oscillations in the vicinity of the stable inter-site configuration. (b) Time variation of the norm of the four central particles. Parameters: $W_1 = -0.012$, $W_2 = 0$, $\omega = -0.99$, which corresponds to the point A in Fig. 3.

be a hyperbolic point which happens only if the roots $z_{1,2}$ are real, i.e., if

$$\beta^2 - 4\gamma^2 > 0. \quad (45)$$

The sign of z specifies the type of the tail solution: $z > 0$ corresponds to the tail decaying monotonically with distance from the soliton's center, while $z < 0$ means that the decaying tail solution oscillates near the carrier solution F .

The absolute value of z characterizes the degree of localization of the tail. If $|z|$ is small, then the tail solution is weakly localized, otherwise it is strongly localized. We found that, in many cases, there is a correlation between the degree of localization of the tail solution and that of the soliton itself.

The tail solution was found from the linearized equation and it can only provide necessary conditions for the existence of a soliton solution. The nonlinear terms, depending on their structure and the values of the corresponding coefficients, can either lead to unbounded solutions or to non-localized solutions, or to the desired bounded and localized soliton solutions.

Having a tail solution one can attempt to construct the corresponding soliton solution. To do so, we use the tail solution defined by Eq. (40) to set the initial values for f_{n-1} and f_n and then find f_{n+1} from Eq. (37), solving the cubic (for $W_2 = 0$) or the quadratic (for $W_1 = 0$) algebraic equation. The proper choice of the integration constants C_{\pm} systematically allows one to obtain equilibrium on-site or inter-site soliton solutions, if they exist [24].

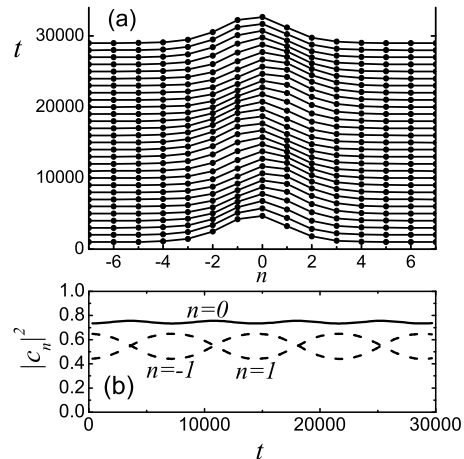


FIG. 7: Pulse in Case 3 ($W_1 = 0$). (a) Space-time evolution of $|c_n(t)|^2$ showing the dynamics of the pulse placed at $t = 0$ asymmetrically with respect to the lattice. The pulse undergoes periodic oscillations in the vicinity of the stable on-site configuration. (b) Time variation of the norm of the central particle and its two nearest neighbors. Parameters: $W_1 = 0$, $W_2 = -0.0136$, $\omega = -0.9704$, which corresponds to the point A in Fig. 5.

To conclude this section we summarize the necessary conditions for the existence of pulses and kinks.

Pulse in Cases 2 and 3. Since the carrying field for pulses with $F = 0$ always exists, there remains only one necessary condition, namely, the condition of the existence of the tail solution of Eq. (45). For $F = 0$ this condition is satisfied for any W_1 and W_2 and for both Cases 2 and 3 when

$$\begin{aligned} \omega > \omega_0 - 2\omega_1 &= -0.73732741 \equiv \omega_a, \\ \omega < \omega_0 + 2\omega_1 &= -0.94041721 \equiv \omega_b. \end{aligned} \quad (46)$$

These conditions simply state that the localized pulses must be located outside the phonon band of the spectrum given by the interval $[\omega_b, \omega_a]$.

The necessary conditions of the existence of a kink include the condition of the existence of the carrier field with $F^2 > 0$, Eq. (38), the stability condition for the carrier field, Eq. (39), and condition Eq. (45) of the existence of the tail solution.

Kink in Case 2. All three necessary conditions are satisfied when $W_1 > 0$ and $\omega_b < \omega < \omega_a$, and they are not satisfied simultaneously for $W_1 < 0$.

Kink in Case 3. All three necessary conditions are satisfied when $W_2 > 0$ and $\omega_b < \omega < \omega_0$, while for $W_2 < 0$ they are satisfied for $\omega_0 < \omega < \omega_a$.

We also specify the frequencies at which z changes sign. In the Case 2 the frequencies are

$$\begin{aligned} \omega_0 - (2/3)\omega_1 &= -0.80502401 \equiv \omega_c, \\ \omega_0 + (2/3)\omega_1 &= -0.87272061 \equiv \omega_d, \end{aligned} \quad (47)$$

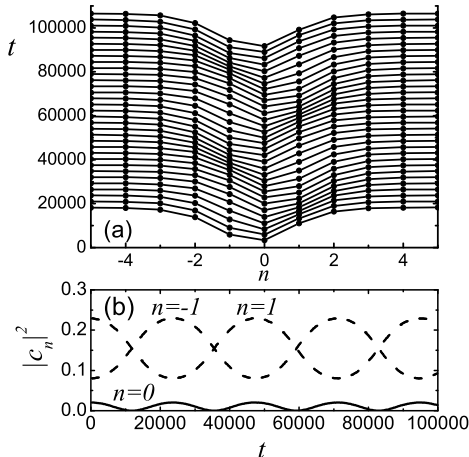


FIG. 8: Kink in Case 2 ($W_2 = 0$). (a) Space-time evolution of $|c_n(t)|^2$ showing the dynamics of the kink placed at $t = 0$ asymmetrically with respect to the lattice. The kink undergoes periodic oscillations in the vicinity of the stable on-site configuration. (b) Time variation of the norm of the central particle and its two nearest neighbors. Parameters: $W_1 = 0.012$, $W_2 = 0$, $\omega = -0.9$, which corresponds to the point B in Fig. 3.

while in the Case 3 they are

$$\begin{aligned}\omega_0 - \omega_1 &= -0.78809986 \equiv \omega_e, \\ \omega_0 + \omega_1 &= -0.88964476 \equiv \omega_f.\end{aligned}\quad (48)$$

B. Soliton solutions

It is well-known [19, 21] that the standard DNLS equation (21) possesses multiple branches of localized solutions which are parametrized by the frequency detuning outwards the phonon band. Multiple branches of the stationary localized solutions were also obtained in a different model in the presence of both linear and nonlinear lattices [7]. This allows one to conjecture that any of the lattices introduced in Sec. II should also possess multiple branches of the localized solutions and kinks (discrete dark solitons). Although a thorough study of each of the cases is by itself a nontrivial problem that requires lengthy considerations, to present a panoramic view of the possible nonlinear modes in the above lattices, in the present paper we restrict our study to some representative examples, referring, in most cases, to the lowest branches.

Case 2 ($W_2 = 0$).

For the nonlinearity of the Case 2, using the method described in Sec. VA, we obtain examples of localized solutions of the Eq. (35), namely: pulse, staggered pulse, kink, staggered kink, wave (an anti-dark structure in the form of an oscillatory wave on a non-zero

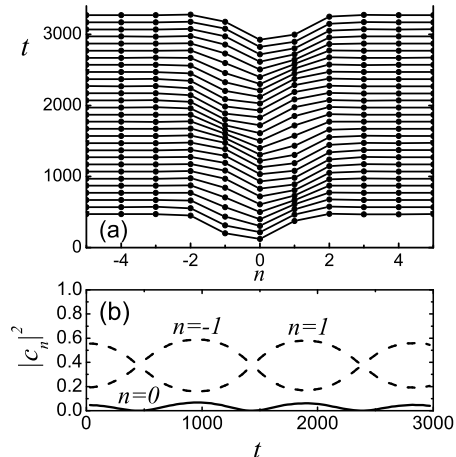


FIG. 9: Kink with oscillatory tail in Case 3 ($W_1 = 0$). (a) Space-time evolution of $|c_n(t)|^2$ showing the dynamics of the kink with oscillatory tail placed at $t = 0$ asymmetrically with respect to the lattice. The kink with oscillatory tail undergoes periodic oscillations in the vicinity of the stable on-site configuration. (b) Time variation of the norm of the central particle and its two nearest neighbors. Parameters: $W_1 = 0$, $W_2 = 0.0136$, $\omega = -0.88$. The kink with oscillatory tail has frequency close to $\omega_f = -0.8896$ and it becomes unstable far from this line (see Fig. 15).

background), and staggered wave. The non-staggered solutions are presented in Fig. 2 for such a parameters: (a) $W_1 = -0.0112$, $\omega = -0.99$, (b) $W_1 = 0.0112$, $\omega = -0.9$, (c) $W_1 = 0.0112$, $\omega = -0.75$. The corresponding staggered solutions can be constructed using the staggering transformation, described above. On-site equilibrium structures are shown but one can also obtain the inter-site ones.

In Fig. 3, the regions of existence of various solutions are indicated on the parameter plane (W_1, ω). Solutions presented in Fig. 2 (a) to (c) have parameters shown by dots marked by the capital letters A to C, respectively. Recall that pulses can exist in the two frequency ranges, $\omega < \omega_b$ and $\omega > \omega_a$, for any W_1 . However, they were found only for $W_1 < 0$, while for $W_1 > 0$ the iterations initiated by the tail solution resulted in unbounded structures. In the portion of the plane with $W_1 > 0$ and $\omega_b < \omega < \omega_c$ kinks [see Fig. 2 (b)] and staggered waves were obtained. On the other hand, in the portion with $W_1 > 0$ and $\omega_d < \omega < \omega_a$, we could construct staggered kinks and waves [see panel (c) of Fig. 2]. It is important to note that $|z|$ is close to 1 near the lines $\omega = \omega_a$ and $\omega = \omega_b$, where pulses, kinks, and waves were found to be wide; z diverges (or vanishes) at $\omega = \omega_c$ for staggered carrier field and at $\omega = \omega_d$ for non-staggered carrier field; in the range of $\omega_d < \omega < \omega_c$, z is always negative and close to 0, resulting in rapidly oscillating or sharply localized (and typically unstable) solutions found from the

tail construction.

Case 3 ($W_1 = 0$).

In the Case 3, three examples of the non-staggered stationary soliton solutions presented in Fig. 4 were found. Shown are: (a) pulse, (b) kink, and (c) kink with oscillatory tail, referred to as oscillatory kink. On-site structures are presented here, but inter-site ones can also be constructed. Model parameters corresponding to panels (a) to (c) of Fig. 4 are depicted by dots in Fig. 5 marked by the capital letters A to C, respectively. Parameters for the non-staggered solutions are: (a) $W_2 = -0.0136$, $\omega = -0.9704$, (b) $W_2 = 0.0136$, $\omega = -0.9$, (c) $W_2 = 0.0136$, $\omega = -0.85$, while the corresponding staggered solutions, as in the Case 2, can be obtained using the staggering transformation.

The pulse tail solution (with $z > 0$) exists for $\omega < \omega_b$ but the pulse itself exists in this region only for $W_2 < 0$, while for positive W_2 we obtained unbounded solutions. Similarly, the staggered pulse tail solution (with $z < 0$) exists for $\omega > \omega_a$ but the staggered pulse itself exists in this region only for $W_2 > 0$, while negative W_2 leads to unbounded solutions.

The kink exists for $W_2 > 0$ and $\omega_b < \omega < \omega_f$, while the staggered kink for $W_2 < 0$ and $\omega_e < \omega < \omega_a$. Finally, the oscillatory kink exists for $W_2 > 0$ and $\omega_f < \omega < \omega_0$, while oscillatory staggered kink for $W_2 < 0$ and $\omega_0 < \omega < \omega_e$.

In Fig. 6 and Fig. 7 we contrast the behavior of pulses in Cases 2 and 3, respectively. In both figures (a) shows the space-time evolution of $|c_n(t)|^2$, while (b) shows time variation of the norm of the central particles. On purpose, we did not optimize the choice of C_{\pm} to get equilibrium on-site or inter-site solutions. As a result, the ensuing profiles are non-stationary and, due to the presence of the Peierls-Nabarro potential, they oscillate in the vicinity of stable configurations. It turns out that in the Case 2 (Case 3) the inter-site (on-site) configuration is stable. This conclusion will be confirmed in Sec. V C. This illustrates the interesting phenomenon of potential inversion of stability (cf. [10]) in comparison with the standard DNLS mode [14]. Parameters in Fig. 6 are: $W_1 = -0.012$, $W_2 = 0$, $\omega = -0.99$, which corresponds to the point A in Fig. 3. Parameters in Fig. 7 are: $W_1 = 0$, $W_2 = -0.0136$, $\omega = -0.9704$, which corresponds to the point A in Fig. 5.

Similar results for dark solitons are presented in Fig. 8 (kink in Case 2) and Fig. 9 (kink with oscillatory tail in Case 3). One can see that in both cases the on-site structures are stable and this will be confirmed in Sec. V C. Parameters in Fig. 8 are: $W_1 = 0.012$, $W_2 = 0$, $\omega = -0.9$, which corresponds to the point C in Fig. 3. Parameters in Fig. 9 are: $W_1 = 0$, $W_2 = 0.0136$, $\omega = -0.88$.

C. Stability of soliton solutions

Let us now study the stability of the stationary soliton solutions of the form of Eq. (36) described in Sec.

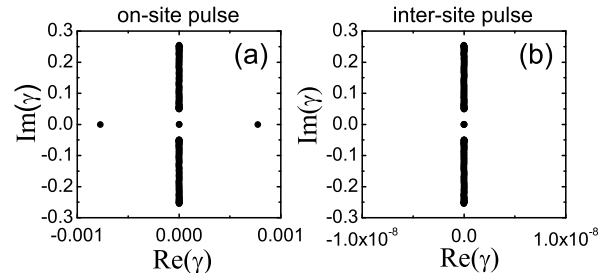


FIG. 10: Spectra of (a) unstable on-site and (b) stable inter-site pulses. The parameters (Case 2): $W_1 = -0.012$, $W_2 = 0$, $\omega = -0.99$ correspond to the point A in Fig. 3.

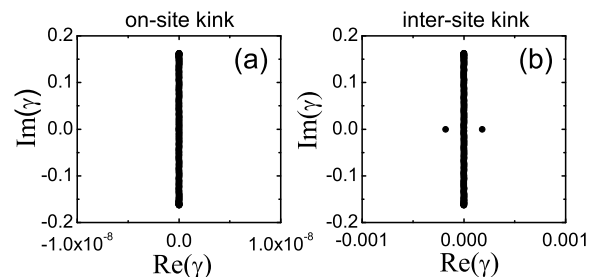


FIG. 11: Spectra of (a) stable on-site and (b) unstable inter-site kinks. The parameters (Case 2): $W_1 = 0.012$, $W_2 = 0$, $\omega = -0.9$ correspond to the point B in Fig. 3.

V B. We consider the following perturbed form of the solutions,

$$c_n(t) = [f_n + \epsilon_n(t)] e^{-i\omega t}, \quad (49)$$

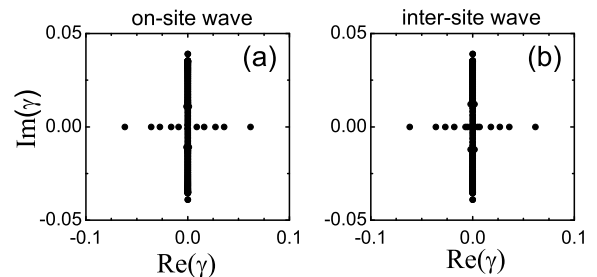


FIG. 12: Spectra of (a) unstable on-site and (b) unstable inter-site wave. The parameters (Case 2): $W_1 = 0.012$, $W_2 = 0$, $\omega = -0.75$ correspond to the point C in Fig. 3.

where the small complex perturbation $\epsilon_n(t)$ is expressed as follows,

$$\epsilon_n(t) = a_n(t) + ib_n(t). \quad (50)$$

Substituting Eq. (49) into Eq. (10) we find that $\epsilon_n(t)$ is governed by the following linearized equation,

$$\begin{aligned} i\dot{\epsilon}_n &= (\omega_0 - \omega)\epsilon_n + \omega_1(\epsilon_{n-1} + \epsilon_{n+1}) \\ &+ W_1 \left[f_{n-1}^2 Z_{n-1} + 2f_n(f_{n-1} + f_{n+1})Z_n \right. \\ &\quad \left. + f_{n+1}^2 Z_{n+1} + f_n^2(Z_{n-1} + Z_{n+1}) \right] \\ &+ W_2 \left[2f_n f_{n-1} Z_{n-1} + (f_{n-1}^2 + f_{n+1}^2)Z_n \right. \\ &\quad \left. + 2f_n f_{n+1} Z_{n+1} \right], \end{aligned} \quad (51)$$

where $Z_n = 3a_n + ib_n$. Then, separating real and imaginary parts of Eq. (51) we derive the following system,

$$\begin{pmatrix} \dot{\mathbf{b}} \\ \dot{\mathbf{a}} \end{pmatrix} = \begin{pmatrix} 0 & \mathbf{K} \\ \mathbf{J} & 0 \end{pmatrix} \begin{pmatrix} \mathbf{b} \\ \mathbf{a} \end{pmatrix}, \quad (52)$$

where vectors \mathbf{a} and \mathbf{b} contain a_n and b_n , respectively, while the nonzero coefficients of matrices \mathbf{K} and \mathbf{J} are given by,

$$\begin{aligned} K_{n,n-1} &= -\omega_1 - 3W_1(f_{n-1}^2 + f_n^2) - 6W_2 f_{n-1} f_n, \\ K_{n,n} &= \omega - \omega_0 - 6W_1 f_n (f_{n-1} + f_{n+1}) \\ &\quad - 3W_2 (f_{n-1}^2 + f_{n+1}^2), \\ K_{n,n+1} &= -\omega_1 - 3W_1(f_n^2 + f_{n+1}^2) - 6W_2 f_n f_{n+1}, \\ J_{n,n-1} &= \omega_1 + W_1(f_{n-1}^2 + f_n^2) + 2W_2 f_{n-1} f_n, \\ J_{n,n} &= \omega_0 - \omega + 2W_1 f_n (f_{n-1} + f_{n+1}) \\ &\quad + W_2 (f_{n-1}^2 + f_{n+1}^2), \\ J_{n,n+1} &= \omega_1 + W_1(f_n^2 + f_{n+1}^2) + 2W_2 f_n f_{n+1}. \end{aligned} \quad (53)$$

In the above expressions, $n = 1, \dots, \mathcal{N}$, where \mathcal{N} is the number of lattice points. For pulses and kinks, we used periodic and anti-periodic boundary conditions, respectively.

A stationary solution is characterized as linearly stable if and only if the eigenvalue problem

$$\begin{pmatrix} 0 & \mathbf{K} \\ \mathbf{J} & 0 \end{pmatrix} \begin{pmatrix} \mathbf{b} \\ \mathbf{a} \end{pmatrix} = \gamma \begin{pmatrix} \mathbf{b} \\ \mathbf{a} \end{pmatrix} \quad (54)$$

results in nonpositive real parts of all eigenvalues γ .

The results of the stability analysis for the equilibrium structures reported in Sec. VB are presented in Figs. 10 to 12 for the Case 2 and in Figs. 13 to 15 for the Case 3. The presented spectra contain (i) the vibration frequencies of the homogeneous background given by Eq. (26); (ii) a pair of zero-frequency modes corresponding to the invariance with respect to the phase shift; (iii) they also can include soliton internal modes falling outside the phonon band, see, e.g., Fig. 14 (a). As was already mentioned, the spectra of stable structures do not possess

eigenvalues with positive real parts, while those of the unstable ones have such eigenvalues. Now we turn to the discussion and comparison of the spectra in the Cases 2 and 3.

Case 2 ($W_2 = 0$).

Spectra of the on-site and inter-site pulses are presented in Fig. 10 (a) and (b), respectively. Interestingly, the inter-site configuration is stable while the on-site one is unstable. This type of instability is typical for the discrete system with Peierls-Nabarro potential, although in the standard cubic onsite nonlinearity case, the results are entirely reversed in comparison to the present case [14] (e.g., the on-site pulse is stable, while the inter-site features a real eigenvalue pair). This indicates that the Case 2 nonlinearity results in the shape of the Peierls-Nabarro potential having a maximum (minimum) for the on-site (inter-site) pulses. Notice that as discussed in [10], such inversions of stability may occur in such generalized models, upon varying their relevant parameters (such as W_1 in the present case). We will see that for the Case 3 nonlinearity the situation for the pulse is exactly the opposite. The parameters used in this case are $W_1 = -0.012$, $W_2 = 0$, $\omega = -0.97$, corresponding to the point A in Fig. 3.

Figure 11 shows results for the kink structures: the on-site kink in (a) is stable while the inter-site one in (b) is unstable. Here the location of maxima and minima of the Peierls-Nabarro potential is the same as in the classical discretization. The parameters $W_1 = 0.012$, $W_2 = 0.0$, $\omega = -0.9$ correspond to the point B in Fig. 3.

Finally, in Fig. 12 we show that (a) the on-site wave and (b) the inter-site wave are both unstable. The parameters $W_1 = 0.012$, $W_2 = 0$, and $\omega = -0.75$ correspond to the point C in Fig. 3.

Case 3 ($W_1 = 0$).

Results of the stability analysis are presented in Figs. 13-15 for the three soliton solutions displayed in panels (a) to (c) of Fig. 4, respectively. The left panels show the spectra of the on-site structures and the right panels show the same for the corresponding inter-site structures. One can see that, in contrast to the Case 2, where the inter-site pulse was found to be stable, in the Case 3 the inter-site structures are always unstable (this is analogous to the case of the standard cubic discrete model with the on-site nonlinearity). This indicates that in the Case 3, the on-site (inter-site) structures are situated in the wells (on the peaks) of the Peierls-Nabarro potential. On the other hand, panels (a) in Fig. 13 to Fig. 15 present purely imaginary spectra for the on-site configurations, and this indicates that, for the corresponding values of model parameters, all three types of equilibrium solutions are stable. However, in Fig. 15 we demonstrate that the on-site configuration of the oscillatory kink is stable at $\omega = 0.88$ [see panel (a)] but it can become unstable e.g. at $\omega = 0.85$ [see panel (c)] with other parameters being unchanged and equal to $W_1 = 0$, $W_2 = 0.0136$.

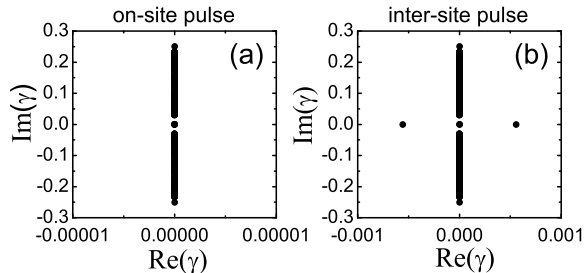


FIG. 13: Spectra of (a) stable on-site and (b) unstable inter-site pulses. Oscillatory motion of the pulse in the vicinity of the on-site configuration is shown in Fig. 6. The parameters (Case 3) $W_1 = 0$, $W_2 = -0.0136$, $\omega = -0.9704$ correspond to the point A in Fig. 5.

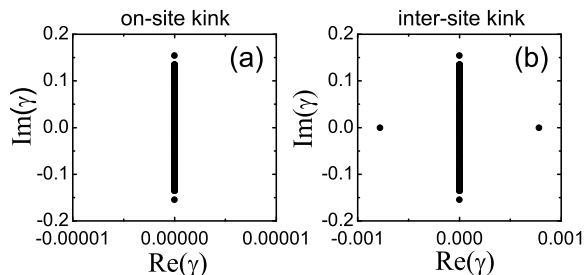


FIG. 14: Spectra of (a) stable on-site and (b) unstable inter-site kinks. The parameter values (Case 3) $W_1 = 0$, $W_2 = 0.0136$, $\omega = -0.9$ correspond to the point B in Fig. 5.

VI. CONCLUSIONS

In this work, we have illustrated the potential for formulation of a rich variety of tight-binding nonlinear lattice dynamical models, stemming from the complex interplay of linear and nonlinear periodic potentials in the Gross-Pitaevskii equation. We have examined various particular possibilities, including quasi-linear models, as well as strongly nonlinear models where the nature of the coupling between the neighbors is itself nonlinear. Furthermore, in the nonlinear ones among our models we have studied the potential for the existence and stability, as well as the dynamics of localized solutions. More specifically, we have reported that the discrete model of Eq. (35) with $W_1 \neq 0$, $W_2 = 0$ (Case 2), and $W_1 = 0$ and $W_2 \neq 0$ (Case 3) supports a number of localized stationary solutions depicted in Fig. 2 and Fig. 4. Interestingly, the nonlinearity of the Case 2 results in stable *inter-site* pulse and stable *on-site* kink (both in staggered and non-staggered forms). On the other hand, the nonlinearity of the Case 3 supports only *on-site* stable localized solutions of three different types, namely, pulses, kinks,

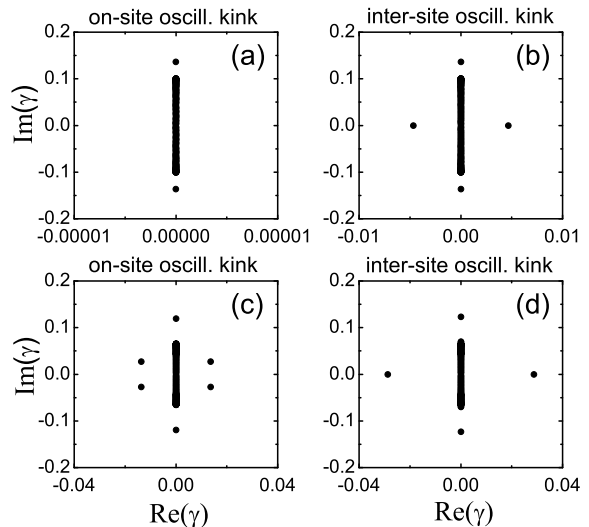


FIG. 15: The top panels show spectra of (a) stable on-site and (b) unstable inter-site oscillatory kinks with $\omega = -0.88$. The bottom panels show the same for $\omega = -0.85$ when both on-site and inter-site oscillatory kinks become unstable. Note that the type of instability in (c) is different from that in (d). In (c) there are two pairs of complex-conjugate eigenvalues, while in (d) there is a pair of purely real eigenvalues. The rest of the parameters are (Case 3) $W_1 = 0$, $W_2 = 0.0136$.

and kinks with oscillatory tails (all in both staggered and non-staggered forms). These results suggest that in the discrete models with nonlinear terms including interactions between nearest neighbors the profile of the Peierls-Nabarro potential can change qualitatively depending on the structure of the nonlinear terms and on the type of the coherent structure. In fact, it has been demonstrated that there exists a wide class of non-integrable discrete models of this sort where the Peierls-Nabarro potential is precisely equal to zero and equilibrium stationary solutions can be placed anywhere with respect to the lattice points [22].

A very natural extension of the present work would be to consider similar types of reductions in higher dimensional settings and to examine in detail the particular localized solutions that may emerge in the resulting lattice models. In particular, higher dimensionality may offer the potential for solutions with topological charge; it would therefore be relevant to examine under what conditions such solutions may be stable and how the relevant results relate to the original continuum model.

Acknowledgments

YVB was supported by the FCT grant SFRH/PD/20292/2004. The work PGK is supported by NSF-DMS-0505663 and NSF-DMS-0619492, and NSF-

CAREER and by the University of Massachusetts. VVK acknowledges support from Ministerio de Educación y Ciencia (MEC, Spain) under the grant SAB2005-0195.

The work of YVB and VVK was supported by the FCT and European program FEDER under the grant POCI/FIS/56237/2004.

-
- [1] O. Madelung, Introduction to Solid State Theory (Springer-Verlag, Berlin, 1978).
- [2] D. N. Christodoulides and R. I. Joseph, *Opt. Lett.* **13**, 794 (1988).
- [3] V. A. Brazhnyi and V. V. Konotop, *Mod. Phys. Lett. B* **18**, 627 (2004).
- [4] O. Morch and M. Oberthaler, *Rev. Mod. Phys.* **78**, 179 (2006).
- [5] G. Fibich, Y. Sivan, M. I. Weinstein, *Physica D* **217**, 1 (2006); Y. Sivan, G. Fibich, M. I. Weinstein, *Phys. Rev. Lett.* **97**, 193902 (2006).
- [6] F. K. Abdullaev and J. Garnier, *Phys. Rev. A* **72**, 061605 (2005); G. Teocharis, P. Schmelcher, P. G. Kevrekidis, and D. J. Frantzeskakis, *Phys. Rev. A* **72**, 033614 (2005); J. Garnier and F. K. Abdullaev, *Phys. Rev. A* **74**, 013604 (2006); H. Sakaguchi and B. Malomed, *Phys. Rev. E* **72**, 046610 (2005); *Phys. Rev. E*, **73**, 026601 (2006); J. Belmonte-Beitia, V. M. Pérez-García, V. Vekslerchik, P. Torres, *Phys. Rev. Lett.* **98**, 064102 (2007); F.Kh. Abdullaev, A.A. Abdumalikov, and R.M. Galimzyanov, *Phys.Lett. A* **367**,149 (2007).
- [7] Yu. V. Bludov and V. V. Konotop, *Phys. Rev. A* **74**, 043616 (2006).
- [8] G. L. Alfimov, P.G. Kevrekidis, V. V. Konotop, and M. Salerno, *Phys. Rev. E* **66**, 046608 (2002).
- [9] V. V. Konotop and S. Takeno, *Phys. Rev. B* **55**, 11342 (1997); *Physica D* **113**, 261 (1998).
- [10] M. Öster, M. Johansson, and A. Eriksson, *Phys. Rev. E* **67**, 056606 (2003).
- [11] M. Öster, Yu. B. Gaididei, M. Johansson, and P. L. Christiansen, *Physica D* **198**, 29 (2004).
- [12] A. Smerzi and A. Trombettoni, *Phys. Rev. A* **68**, 023613 (2003); C. Menotti, A. Smerzi, and A. Trombettoni, *New J. Phys* **5**, 112 (2003).
- [13] W. Kohn, *Phys. Rev.* **115**, 809 (1959).
- [14] P.G. Kevrekidis, K.Ö. Rasmussen and A.R. Bishop, *Int. J. Mod. Phys. B* **15**, 2833 (2001).
- [15] Yu. S. Kivshar and M. Salerno, *Phys. Rev. E* **49**, 3543 (1994).
- [16] V. V. Konotop and S. Takeno *Phys. Rev. E* **60**, 1001 (1999).
- [17] F.Kh. Abdullaev, S.A. Darmanyan, and J. Garnier, *Prog. in Opt.*, **42**, 301 (2002).
- [18] V. V. Konotop and M. Salerno, *Phys. Rev. E* **55**, 4706 (1997); *ibid* **56**, 3611 (1997); V. V. Konotop, *Chaos, Solitons & Fractals*, **11**, 153 (2000).
- [19] G. L. Alfimov, V. A. Brazhnyi, and V. V. Konotop, *Physica D* **194**, 127 (2004)
- [20] G. L. Alfimov, V. V. Konotop, and M. Salerno, *Europhys. Lett.* **58**, 7 (2002).
- [21] E. W. Laedke, O. Kluth, and K. H. Spatschek, *Phys. Rev. E* **54**, 4299 (1996).
- [22] P.G. Kevrekidis, S.V. Dmitriev, and A.A. Sukhorukov, *Math. Comput. Simulat.* **74**, 343 (2007); S.V. Dmitriev, P.G. Kevrekidis, N. Yoshikawa, and D.J. Frantzeskakis, *J. Phys. A: Math. Theor.* **40**, 1727 (2007); S.V. Dmitriev, P.G. Kevrekidis, A.A. Sukhorukov, N. Yoshikawa, and S. Takeno, *Phys. Lett. A* **356**, 324 (2006) (see also arXiv nlin.PS/0603047, with corrected misprints); D.E. Pelinovsky, *Nonlinearity* **19**, 2695 (2006).
- [23] The numerical values of the Fourier coefficients, of the Wannier functions and of the overlap integrals, presented in this paper were obtained by the software developed by G. L. Alfimov.
- [24] This is a variant of the shooting method used for obtaining of localized modes in continuous models [3, 7, 19, 20].